GeoHazards

MDPI

Article

Fault Structure Characterization in the Gulf of Evia (Central Greece): Insights from an Enhanced, Relocated Seismic Catalog (2018–2023)

Andreas Karakonstantis [1,2], Vasilis Kapetanidis [1], Nikolaos Madonis [3], Haralambos Kranis [4] and George Kaviris [1,*]

[1] Section of Geophysics-Geothermics, Department of Geology and Geoenvironment, National and Kapodistrian University of Athens, 15784 Athens, Greece; akarakon@geol.uoa.gr (A.K.); vkapetan@geol.uoa.gr (V.K.)
[2] Seismological Laboratory, Department of Geology, University of Patras, 26504 Patras, Greece
[3] National Observatory of Athens, Institute of Geodynamics, Lofos Nymfon, Thission, 11810 Athens, Greece; nicosmadon2@gmail.com
[4] Section of Dynamic, Tectonic and Applied Geology, Department of Geology and Geoenvironment, National and Kapodistrian University of Athens, 15784 Athens, Greece; hkranis@geol.uoa.gr
* Correspondence: gkaviris@geol.uoa.gr

Abstract

We present an enhanced earthquake catalog for Central Evia and the Northern Gulf of Evia, in Central Greece, between June 2018 and November 2023. The area is characterized by a low background seismicity rate, with occasional clustered events and seismic swarms, including those of February–April 2022 near Drosia and of October 2022 near Styra. The seismic catalog was enhanced by integrating additional data acquired through the application of the EQ-Transformer deep-learning model. A total of ~1400 events were analyzed, with ~1200 of them being successfully relocated with the double-difference method. The available focal mechanisms indicate predominantly normal, oblique-normal, and pure strike-slip faulting. The relocated seismicity was examined in conjunction with known mapped faults to investigate the activated structures at depth, providing insight into their degree of activity. In Drosia, the seismicity, at a depth of ~14 km, can be related to an E–W dextral strike-slip fault, with subtle surficial expression. In Psachna, the epicenters are oriented in an NE–SW direction, not matching the strike of the mainshock's normal focal mechanism, but roughly coinciding with NE–SW-oriented topographic spurs and the local drainage pattern. In Markates and Prokopi, the seismicity is sparse, but the focal mechanisms are consistent with SW–NE dextral strike-slip faulting, aligned with the trend of the Nileas depression and the Prokopi–Pelion fault zone. Finally, in Mouriki, the seismic cluster is characterized by WNW-ESE normal faulting, most likely related to the SSW-dipping Messapio fault.

Keywords: earthquake relocation; deep-learning models; strike-slip faults; Gulf of Evia

Check for updates

Academic Editor: Riccardo Caputo

Received: 9 February 2026
Revised: 23 March 2026
Accepted: 27 March 2026
Published: 31 March 2026

Copyright: © 2026 by the authors. Licensee MDPI, Basel, Switzerland. This article is an open access article distributed under the terms and conditions of the Creative Commons Attribution (CC BY) license.

1. Introduction

Evia is an NW–SE elongated island in Central Greece, on the western side of the North Aegean Sea (Figure 1). The broader region hosted two destructive earthquakes on 20 April and 27 April 1894 near Atalanti (Central Greece), with magnitudes of 6.7 and 6.9, respectively, which are both linked to the local fault system [1,2]. Since that time, there have not been any major earthquakes (M > 6.0) in the area, indicating a period of relatively low seismic activity [3]. The neighboring areas were affected by moderate-sized

events on 27 September 1916 (M = 5.7), north of Atalanti, and two M5.0 events on 12 April 1925, south of Prokopi, Evia, and 11 September 1931, in Northern Evia [4]. Recently, the study area has experienced certain seismic sequences that began with the occurrence of shallow earthquakes of M_w 5.1–5.2 on 17 November 2014, in the Northern Gulf of Evia, and continued until the end of the first semester, with another significant event (M_w = 5.2) taking place on 9 June 2015. According to [5], these earthquakes occurred on NW–SE left-lateral strike-slip faults mapped within the Northern Gulf of Evia [6]. The focal depths of these events, located near the area of study, ranged from 8 km to 15 km.

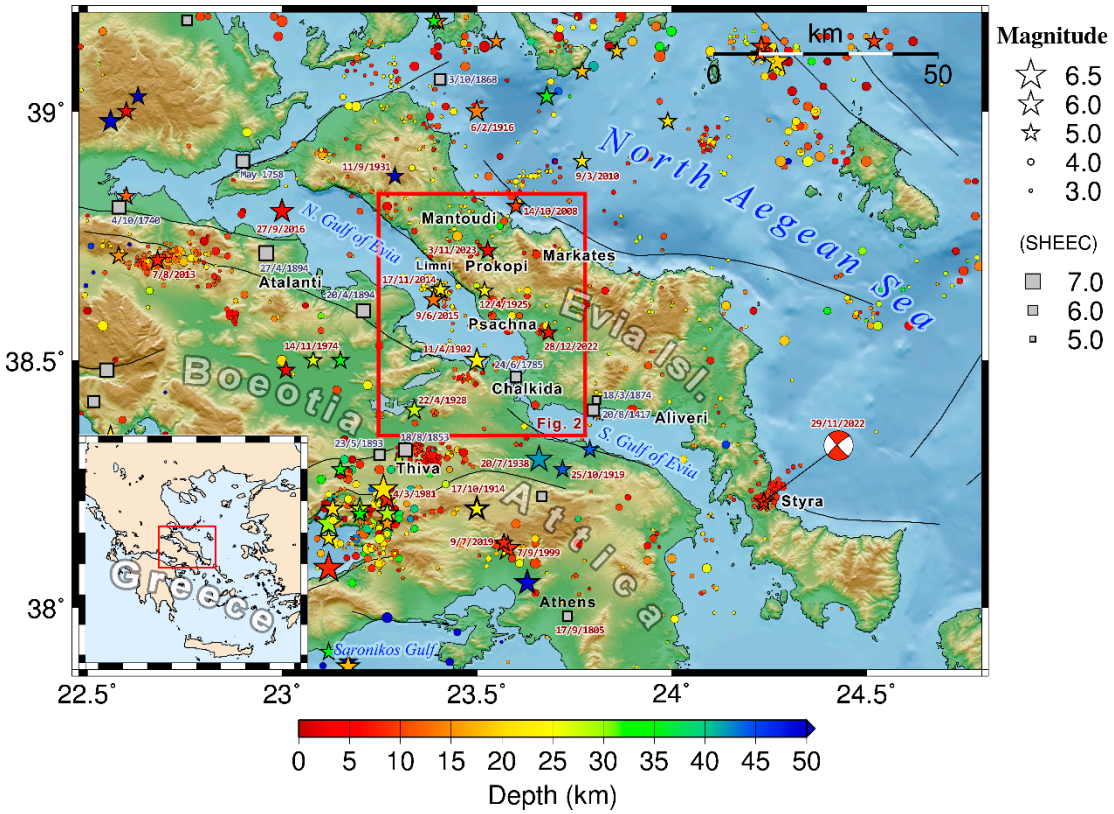


Figure 1. The study area in Central Evia–Northern Gulf of Evia (red rectangle in the inset map of Greece at the lower-left). Historical seismicity (gray squares) is from the SHEEC database [7] for 1000–1899. Instrumental seismicity (circles and stars) is compiled from the catalog of [4] for the years 1900–2009, from the bulletin of the Geodynamics Institute of the National Observatory of Athens [8] and from the database of the Seismological Laboratory of the National and Kapodistrian University of Athens [9]. Events of the instrumental era with a magnitude of M $\geq$ 5.0 are shown with stars. The solid lines depict the fault-source traces from the SHARE database [10,11]. The focal mechanism of the 29 November 2022 M_w = 4.9 event at Styra is from the SL-NKUA database [9].

In early 2022, a rise in the seismicity of the study area was observed. The most significant events occurred on 28 December 2022 (M = 5.0), near the town of Psachna, north of Chalkida, and on 3 November 2023 (M = 5.2), a few km west of Markates. In this study, we analyze the seismicity between June 2018 and November 2023 in the study area. We enhanced the available seismological data from manual analysis with additional arrival-time picks generated by a deep-learning model and relocated the hypocenters using the double-difference method. Furthermore, we examine the spatiotemporal distribution of seismicity to investigate possible migration patterns associated with these seismic sequences. We also correlate the spatial patterns of seismicity and the focal mechanisms of major events with mapped surface faults to assess the possible geometries of the structures activated at depth.

The main motivation to conduct this study is that the earthquake sequence, widely felt in the metropolitan area of Athens, occurred in an area characterized by unclear fault kinematics. This uncertainty stems from the absence of well-preserved, striated fault surfaces, which is attributed to the erodible nature of the outcropping fault structures. The lack of direct evidence for slip on the faults complicates the interpretation of their seismotectonic behavior. The development of a more complete catalog of the focal parameters for these sequences (hypocenters and focal mechanisms) aims to provide a clearer understanding of the local seismotectonic setting.

2. Data and Methods

In this work, we analyze the seismicity in Central Evia and the Northern Gulf of Evia between June 2018 and November 2023. Initial catalog and seismic phase arrival-time data were acquired from the database of the Seismological Laboratory of the National and Kapodistrian University of Athens (SL-NKUA) [9], which largely consists of manually analyzed events. The dataset was enhanced by incorporating additional P- and S-wave arrival-time picks, using the deep-learning model EQ-Transformer (EQT; [12]) that is available through the SeisBench (v0.6.1) toolbox of machine-learning tools [13]. For this purpose, we acquired seismic waveform data from local and regional stations of the Hellenic Unified Seismic Network [14]. For the period from September 2022 onwards, additional data from stations that were deployed in the framework of the AdriaArray project [15–17] were processed. An EQT model, pre-trained on the INSTANCE dataset [18], was employed to automatically pick P- and S-wave arrivals in windows around the theoretically expected arrival times for the selected events in the study area. A broad window of ± 2 s was allowed for both P and S candidate EQT picks, which is especially useful when the initial available phases are automatic P-wave arrival times that are routinely derived by a simple STA/LTA method. An additional constraint was set for a minimum allowed an S-P arrival-time difference of 0.2 s for each station, mainly to avoid possible misidentified S phases. The acquired picks from the EQT model were added to the data when arrivals were missing or when manual picks were unavailable in the original dataset (see Figures S1e and S2e for a comparison of the number of phases between the initial and the enhanced dataset). Weight classes were assigned according to the probability values yielded by EQT for each of the P- and S-wave arrival-time picks (see Table S3).

The initial locations of the data were determined by using a regional velocity model [19]. Further filtering was performed to ensure that events were located more accurately in the database. This involved an application of a minimum 1D velocity model inversion, using the mean travel-time residuals and location errors (RMS, ERX, ERY, and ERZ) minimization, based on the method proposed by [20,21]. The initial phase data were then filtered by selecting earthquakes with at least eight (8) P-wave and five (5) S-wave arrival times, with a maximum azimuthal gap of 180°. In total, a dataset of 540 events was created. The selected seismic phases were obtained by stations within an epicentral distance of ~200 km, excluding the Pn and Sn phases. Subsequently, the optimal solution involved multiple iterations per layer (velocity and ceiling depth), starting from the initial 1-D velocity model. A gradual reconstruction of the final 1D velocity structure was performed by evaluating misfit functions (RMS, ERH, and ERZ) over a range of ceiling depths and velocity values. The robustness of each model was carefully tested by conducting several HypoInverse (v1.1) [22] runs and calculating the resulting error, including variations in the number of layers and their ceiling depth. The option of applying a 1D model was favored over a 3D one, mainly due to its simplicity and the speed of routine operations, while the accuracy of the earthquake locations was not far behind, given the limited lateral variance and a fair station distribution in the available dataset.

3. Results

The final dataset consists of 1416 earthquakes (Figure 2a) located using the HypoInverse code, employing the aforementioned local 1D velocity model for the area of Northern Gulf of Evia-Boeotia (Table 1), close to the region of the Thiva 2020–2021 earthquake sequence [23,24]. Given that seismicity involves distinct, well-separated structures, we grouped hypocenters into 8 spatial groups before further processing. The initial clustering was performed by applying Ward's linkage on a matrix of the 2D inter-event distances, and the final groups were formed by merging smaller sub-clusters after a visual inspection. Formal location uncertainties and other statistics are presented in Figure S1, and the average values for each group are reported in Table S1, while a comparison with the initial phases' dataset is presented in Figure S2, Table S2 and Figure S3, respectively (see Supplementary Materials). The median RMS travel-time residual is slightly increased in the enhanced dataset (from 0.17 s to 0.22 s), as the addition of more phases, especially S, tends to increase the travel-time residuals, whereas the horizontal and vertical location uncertainties have been reduced by 20–25% (mean ERH from 0.60 km to 0.44 km and median ERZ from 2.16 km to 1.74 km). The median azimuthal gap is also reduced by ~25%, from 112° to 85°. The EQT-enhanced dataset does not cause any observable bias to the solutions but rather concentrates several spatial clusters and reduces the scattering of the spatial distribution (Figure S4). Small improvements can also be observed in the depth distribution, with scattered events at shallow depths getting more concentrated towards spatial clusters at slightly larger depths (Figures S5–S8), with the median depth increased from 8.08 km to 8.73 km in the EQT-enhanced dataset.

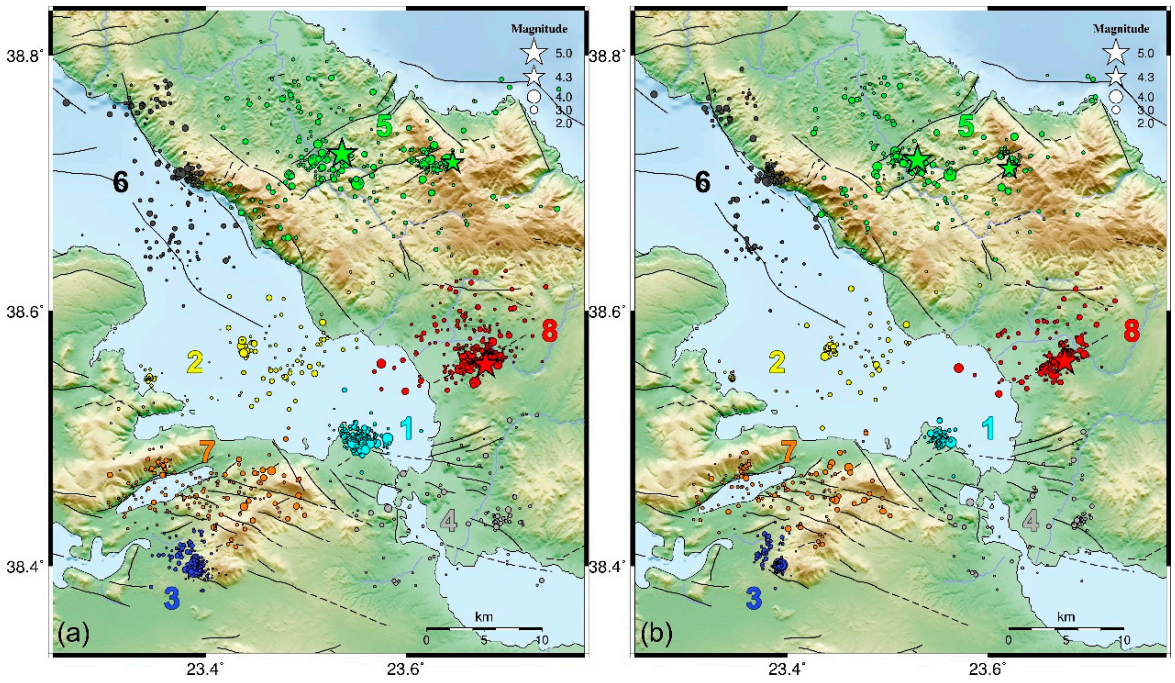


Figure 2. Seismicity in Central Evia–Northern Gulf of Evia, between June 2018 and November 2023. (**a**) Initial locations acquired using HypoInverse [22], employing the enhanced dataset (including additional arrival-time data acquired using EQ-Transformer), (**b**) epicenters relocated with the double-difference method (HypoDD). Colors and numbers represent the 8 spatial groups. Events with magnitude $M_L \geq 4.3$ are presented with stars. Fault traces are after [5,25–31], with additions from the present study.

Table 1. Local 1D P-wave velocity model for the area of the Northern Gulf of Evia-Boeotia ($Vp/Vs = 1.76$).

Layer	*Vp* (km/s)	Depth (km)
1	5.0	0
2	5.9	4
3	6.2	8
4	6.8	29
5	7.9	42

To improve the relative locations of correlated events, we applied the double-difference method, using the HypoDD (v2.1) code [32]. This algorithm works on the assumption that when the distance between two hypocenters is much smaller than their raypath length to a station, then differences in the observed travel-times can be attributed to their inter-event separation. The double-difference method reduces errors caused by an unmodeled velocity structure, including lateral heterogeneities, as well as inconsistencies in arrival-time picking. For this purpose, we measured differential arrival times by cross-correlating the waveform recordings of closely spaced events. Initially, a correlation matrix was formed by combining measurements of the cross-correlation maximum (XC_{max}) from full signal waveforms filtered between 2 Hz and 11 Hz at selected stations in the study area. This ensures that long-period trends and high-frequency noise are filtered out to enable cross-correlation of small earthquake recordings at local to regional distances (e.g., [24,33]). For each event pair, the maximum of the individual XC_{max} results from all stations was retained in the combined matrix. Nearest-neighbor linkage was applied and 148 multiplets, containing 925 events, were formed with an optimal threshold value of 0.68, which maximizes the difference between the size of the largest cluster and the number of clustered events [34] (see also Figures S9 and S10 in Supplementary Materials). Afterwards, cross-correlation was performed for all combinations of event pairs within each multiplet for the P- and S-wave windows at each station, using the available arrival-time picks for the respective phases. The XC_{max} value and the corresponding time delay were registered to be incorporated in the cross-correlation data and the catalog data for HypoDD.

The double-difference relocation was performed separately for each spatial group to facilitate the procedure and avoid links between unrelated clusters. The inversion was performed in two stages, first with stronger weights for the catalog data and then switching to higher weights for the cross-correlation data, to enhance the relative locations between the strongly correlated events, forming tighter sub-clusters. A total of 1203 events (~85% of the initial catalog) were successfully relocated. After the relocation procedure, the clustered events become more concentrated around their centroid, and scattering in the distribution of epicenters is reduced (Figure 2b). However, it is noted that, despite the tight concentration of some small clusters, their absolute focal depth is poorly constrained. In many cases, the depths appear scattered, creating a quasi-vertical distribution of hypocenters. This is an artifact produced by significant vertical location uncertainties, primarily due to the lack of a local network near the epicentral area. This prohibits the definition of plane geometries at depth and restricts the interpretation to a general range of crustal depths where the seismicity is located.

Seismicity in the study area for the period June 2018–November 2023 is relatively low, except for short-lived bursts, either triggered by a main event or in the context of a seismic swarm. The magnitude of completeness of the catalog is $M_c = 1.8$. Figure 3 shows a histogram of the number of events per 15 days at the top, stacked by spatial group, while the bottom panel presents the cumulative number of events per spatial group for events with $M \geq M_c = 1.8$. In the more active groups, the average background seismicity rate

ranges from 0.5 to 0.8 events per month. The seismicity rate abruptly increased at specific dates, as indicated by the arrows. The statistical significance of the observed rate increases is tested using the beta-statistic of [35] (see Supplementary Materials).

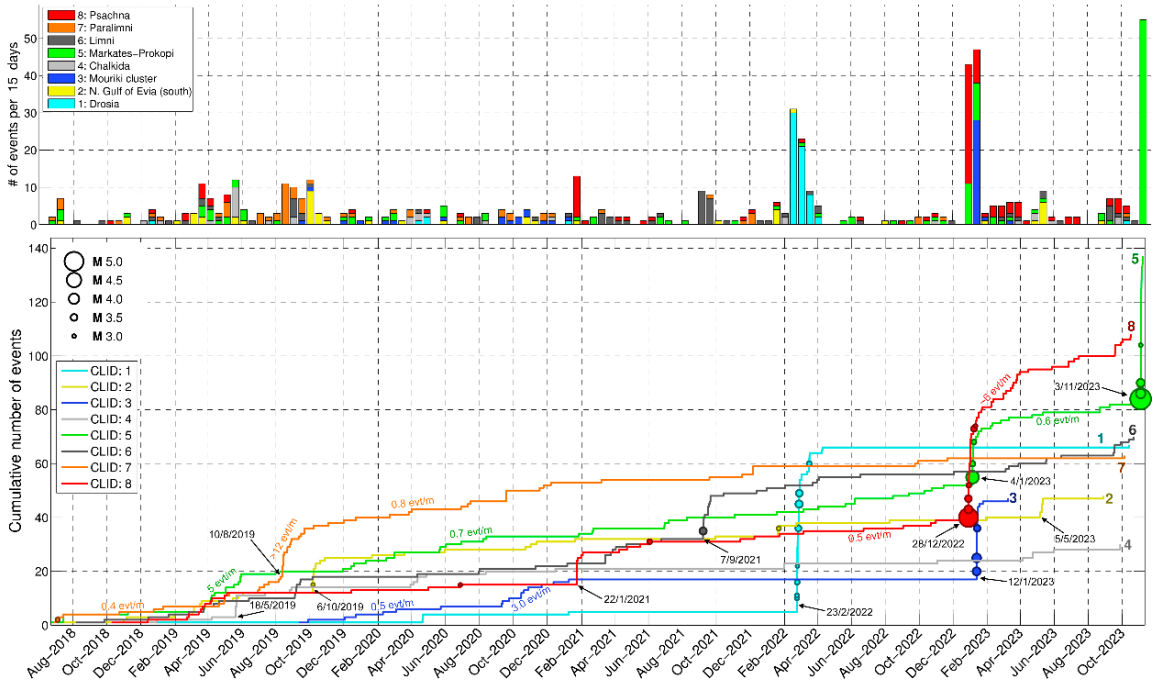


Figure 3. (**Top**) Stacked histogram of the number of events per 15 days; (**Bottom**) cumulative number of events, with $M \geq M_c = 1.8$. The colors represent the 8 spatial groups between which seismicity has been distributed. Seismicity rates are reported in events per month (evt/m). Dates of initiation of bursts in the seismicity rate in specific clusters are marked with arrows. Events with $M_L \geq 3.0$ are drawn as circles.

A small spike in the seismic activity was observed between 19 and 21 May 2019 in the sparse group #4 (gray; Figure 2b), near Chalkida, where two events of $M_L = 2.5$ and 2.6 occurred on 20 and 21 May, respectively. Group #7 (orange), with scattered seismicity in mainland Greece, at the southern shores of the Northern Gulf of Evia, presented an increase in its seismicity rate, starting on 12 August 2019, without being triggered by any significant event. This burst in seismic activity followed the $M_w = 5.1$ event of 19 July 2019 at Mt. Parnitha, ~20 km NW of Athens [36,37]. The largest event during that time in group #7 was an $M_L = 2.2$ event on 18 August 2019. Also, it has been preceded by a lower, but significant, rate increase that started around 11 April 2019. On 6–7 October 2019, a small burst of activity occurred in group #2 (yellow), in the southern part of the Northern Gulf of Evia, including two events with magnitudes of 2.9 and 3.0. Very low seismicity rates were observed during 2020. An increase in the seismicity rate of group #8 (red) began on 22 January 2021 near Psachna, including an $M_L = 3.0$ event on 23 January and two more events with magnitudes of 2.8 and 2.9 on the same day. The unrest lasted until about 3 February 2021. A burst of seismicity in group #6 (black), near Limni (Figure 1), was triggered by an $M_L = 3.6$ event on 7 September 2021, which was preceded by a few smaller events.

A seismic swarm began on 23 February 2022 at group #1 near Drosia. It was initiated by small events, including several earthquakes with $3.0 \leq M_L \leq 3.4$, and culminated with two events of M_L 3.5–3.6 on 26 and 27 February. The swarm lasted up to early April 2022, with at least two secondary bursts, including one triggered by an $M_L = 3.2$ event on 17 March 2022. This swarm presented strong clustering, with the relocated hypocenters

being concentrated at focal depths of ~14 km (Figure 4). The focal mechanism for an M_w = 3.6 event of the swarm that occurred on 25 February suggests strike-slip faulting in an E–W direction (dextral) or an N–S direction (sinistral). The concentration of group #1 appears to align with the WNW-ESE striking plane, which makes the first scenario (dextral strike-slip fault) more plausible than the second one. On the contrary, the seismicity of the offshore group #2 (yellow) is scattered in a wide range of depths, due to the larger vertical location uncertainties (Table S1). It is worth mentioning that [5] suggested that the 2014–2015 earthquake swarms in the Northern Gulf of Evia were related to the WNW-ESE and NW–SE left-lateral strike-slip faults.

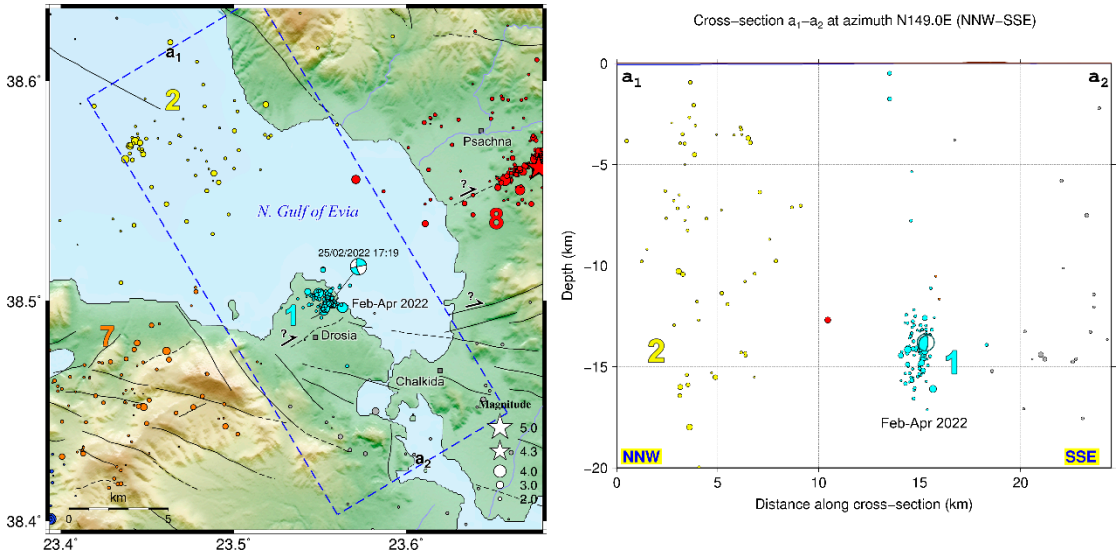


Figure 4. Map and cross-section a_1–a_2 (NNW-SSE) of relocated events between Central Evia and Central Greece, for the period June 2018–November 2023, focused on spatial groups #1 and #2. The location of the February–April 2022 swarm near Drosia is presented. The focal mechanism of the 25 February 2022 event is from the GI-NOA database.

Starting in late October 2022, a very significant swarm evolved in the south of Evia Island, to the southeast of the study area, near Styra (Figure 1) [38,39]. This sequence began with small events on 25 October, but on 29 November, it produced two earthquakes with magnitudes of 4.8 and 4.2 within less than an hour, followed by an M_L = 5.0 earthquake a few hours later. The activity persisted for several months, including five more $M_L \geq 4.0$ events, with the largest (M_L = 4.6) occurring on 22 April 2023. The focal mechanisms of the major events of that seismic swarm indicated strike-slip faulting in a SW–NE direction (dextral) or an NW–SE direction (sinistral).

On 28 December 2022, an M_w = 4.7 event triggered a mainshock–aftershock sequence in group #8 (red), near Psachna. The largest aftershocks occurred on the same day as the mainshock, with magnitudes 3.7 and 3.5. The focal depths of the relocated hypocenters mainly range between 6 km and 11 km, with a median of 7.7 km (Table S1). A local station (HA.PSAH) was installed by SL-NKUA on 11 January 2023 to monitor the local seismicity; however, by then, the aftershock activity had mostly ceased, and no other significant earthquakes have occurred in that area since. The strong scatter in the focal depth distribution prevents the direct definition of the fault geometry. The focal mechanism of this event appears to have a difference from pure E–W normal faulting, giving an additional challenge to interpret the delineation direction (WSW-ENE) of the relocated epicenters (Figure 5).

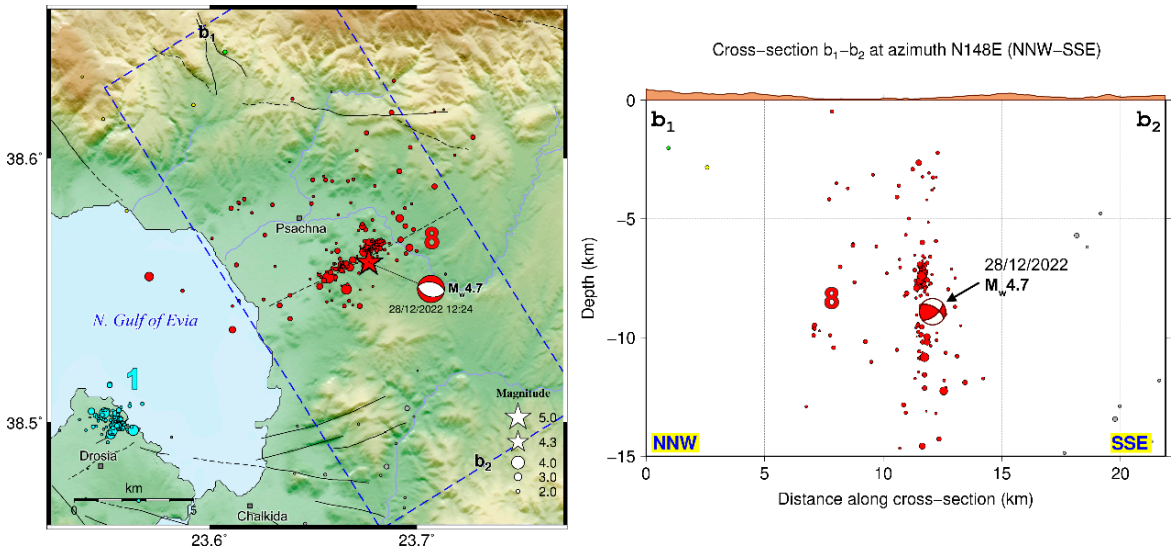


Figure 5. Map and cross-section b_1–b_2 (NNW-SSE) of relocated events near Psachna, Central Evia, between June 2018 and November 2023, focused on spatial group #8. The location of the 28 December 2022 M_w = 4.7 event near Psachna is shown (focal mechanism from the GI-NOA database, with a reported centroid depth of 9 km, in agreement with the relocated hypocenter).

The available focal mechanisms of significant events indicated dominant strike-slip and normal fault kinematics. The February 2022 cluster near Drosia and the October 2022 swarm near Styra both exhibited strike-slip faulting. The depth distribution of hypocenters varied across the spatial groups, with some clusters, such as group #1 near Drosia, concentrated at around 14 km in depth. Other groups, e.g., group #2 in the southern part of the Northern Gulf of Evia, are characterized by a wider range of focal depths, due to the larger vertical location uncertainties. In the area of Psachna, the alignment of the epicenters, along with the focal depth distribution, fits well with a fault that has not been previously mapped (Figure 5).

The seismic activity was observed on 4 January 2023 in group #5 (green), near Markates, including an M_L = 3.6 event at 01:16:16 UTC. This was followed about 19 h later by an M_w = 4.1 event in the same area. The focal mechanism suggests oblique-normal to strike-slip faulting in a SW–NE direction (dextral) or NW–SE direction (sinistral). The aftershock activity, which lasted until 10 January 2023, forms a tight cluster at a depth of 10 km (Figure 6).

On 12 January 2023, another short-lived swarm occurred in the study area, in group #3, near Mouriki. This involved three events: two with magnitudes of 3.8 and 3.7 within less than 2 h, and another M_L = 3.5 event the next day. The hypocenters of this seismic swarm are concentrated at a depth of ~13 km (Figure 7). The shallower part of group #3 seems to be a continuation of the sparse seismicity of group #7. The focal mechanism of the first M_w = 3.8 event of 12 January 2023 indicates normal faulting in a WNW-ESE direction. A small increase in the seismicity rate of group #2 (yellow) occurred between 5 and 11 May 2023, without being associated with any significant earthquake. On 3 November 2023, an M_w = 5.0 triggered a mainshock–aftershock sequence in group #5 (green), near Prokopi (east of Markates). This earthquake appears to have activated a different structure than the one associated with the M_w = 4.1 event on 4 January 2023, west of Markates. However, the focal mechanism of this mainshock is similar to the one of the 4 January event, albeit with a very small normal component.

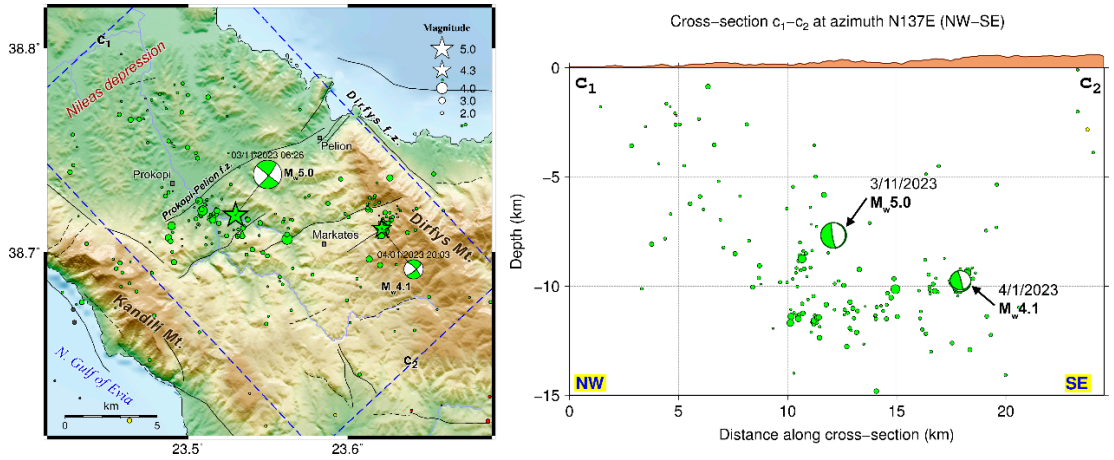


Figure 6. Map and cross-section c_1–c_2 (NW–SE) of relocated events in Central Evia between June 2018 and November 2023, focused on spatial group #5. The locations of the two major events of 4 January (M_W = 4.1, near Markates) and 3 November (M_W = 5.0 near Prokopi) 2023 are presented. The focal mechanisms are from the database of GI-NOA.

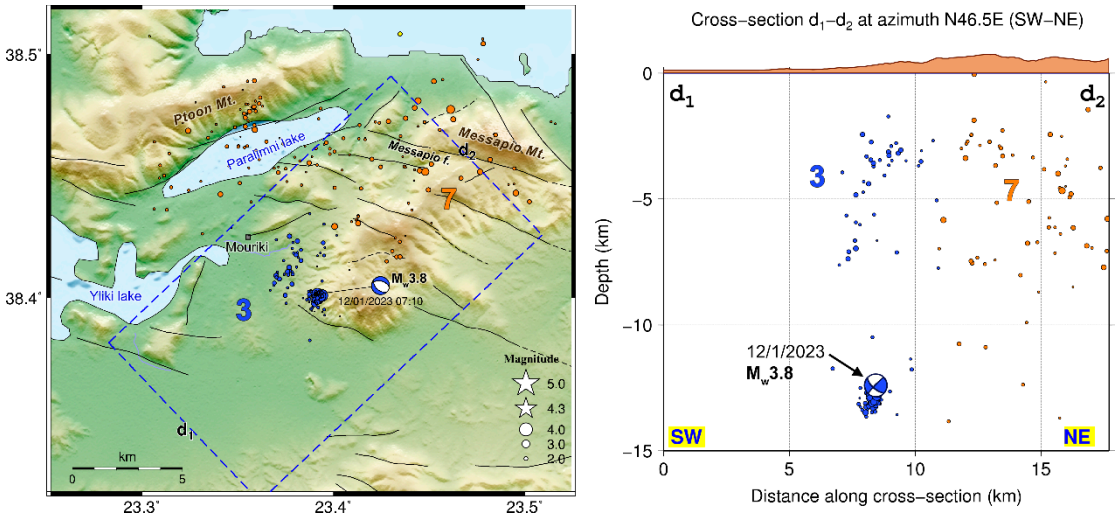


Figure 7. Map and cross-section d_1–d_2 (SW–NE) of relocated events near Mouriki, Central Greece, between June 2018 and November 2023, focused on spatial groups #3 and #7. The location of the 12–13 January 2023 cluster near Mouriki (group #3, blue) is presented. The focal mechanism of the 12 January 2023 M_W = 3.8 event is from the database of SL-NKUA.

4. Discussion

The occurrence of NE–SW oblique-normal and strike-slip faulting has been identified and mapped almost all across Evia Island, as shown in this and previous, older and more recent studies (i.e., [31,39–42]). This occurrence highlights and supports the influence of the westward propagation of the North Anatolian Fault System (NAFS) in the northern and central Aegean, with active deformation becoming more diffuse, expressed through unlinked smaller faults, as appears to be the case in Evia. An exception is probably the NE–SW "Pelagonian Fault" that cross-cuts the southern part of the island, as suggested by [43]. Further south and west of Evia, the namesake North and South Gulfs host evidence of a transtensional deformation style [42], as indicated by the occurrence of oblique-normal E–W to WNW-ESE faulting [41,44] and NW–SE sinistral strike-slip faulting [5]. Within the Greek mainland, although the active deformation is mainly accommodated by E–W-striking normal and oblique-normal faults (such as the Messapion Fault, or the Yliki

Fault [24]), evidence of strike-slip faulting also exists, such as the case of the Elatia 2023 earthquake [42,45].

In this study, we tried to enrich the available earthquake catalog for Central Evia and the Northern Gulf of Evia, focusing on the seismic activity that occurred between June 2018 and November 2023. The background activity was characterized by a low seismicity rate. However, several short-lived clusters and swarms also occurred, including the seismic cluster near Drosia, during February–April 2022, and the seismic swarm near Styra in late October 2022, which contained multiple events with $M_L \geq 3.0$.

In the area of Psachna, the alignment of the epicenters, along with the focal depth distribution, fits well with a fault that has not been previously mapped. The trace of this probable fault is distinguishable through morphology, as it is associated with NE–SW-oriented topographic spurs and the local drainage pattern, with second- and third-order streams that are aligned along this direction (Figure 5). Alternatively, judging by the depth and the focal mechanism of the mainshock alone, it could be related to the (south-dipping) E–W normal fault system that is mapped north of Psachna.

Further to the NE, near Markates (Figure 6), several studies in the area (e.g., [31]) showed that a suite of NE–SW faults can be mapped. The structures form the south-eastern border to the broader area of the "Nileas depression", especially the Prokopi–Pelion fault zone. This feature appears to control the segmentation of the NW–SE Dirfys Fault, which runs along the Aegean coast of Northern Evia (Figure 6). Nonetheless, despite their distinguishable morpho-tectonic characteristics, the kinematics of these faults remain unclear, as they are not associated with clear, striated fault surfaces, owing to the erodible nature of the outcropping geological formations. The concentration of seismicity near Mouriki, along with the determined focal mechanism solutions, seems compatible with the fault grain in the area, where a suite of sub-parallel, WNW-ESE normal faults is mapped. Considering the hypocentral depth and the location of the mainshock, the responsible structure is likely the SSW-dipping normal Messapio fault (Figure 7), which bounds the namesake mountain from the south, with a mappable length of about 13 km.

In the Greek mainland, near Drosia (Figure 7), the seismic activity tends to favor a roughly E–W dextral strike-slip fault. However, there is little, if any, surficial evidence of it, except for two fault-controlled NE–SW fault scarps at the Drosia peninsula. Previous sequences, like the 2013 Taxiarchis (NW Evia), the 2015 offshore Malesina–Kandilli, and the 2022–2023 Psachna events, were linked to NW–SE oblique sinistral faults [5,42]. In contrast, ~E–W to NE–SW striking structures were associated with dextral oblique-slip movement during the 14 October 2008 Mantoudi M_w = 5.1 earthquake [46]. Thus, the occurrence of group #1 earthquakes in either fault plane (E–W or N–S) is plausible (Figure 4). If this is the case, one (or both) of these fault lines could correspond to the westward prolongation of the fault, identified on the opposite side of the gulf, at Psachna.

Overall, the study area shows that the westward influence of the NAFS becomes less pronounced the further we move away from the Aegean Sea domain. This is related to the ongoing propagation of the NAFS, which leads to the re-organization of the pre-existing, inherited tectonic fabric within the continental block of mainland Greece that has controlled the evolution of the rift of the North Gulf of Evia and the adjacent Lokris basin (initiated in the Upper Miocene–Lower Pliocene), where extension is also influenced by the rollback of the subducting African plate [47].

5. Conclusions

The integration of the EQ-Transformer deep-learning model significantly enhanced the earthquake dataset by providing additional P- and S-wave arrival-time picks. In turn, this permitted more accurate initial absolute locations, followed by relocation using the double-

difference method. The latter reduced the horizontal scattering of epicenters, enabling the delineation of seismically activated structures, where possible, mainly in terms of their strike. However, the focal depths cannot be improved without the deployment of local seismological stations in the study area: hence, the geometry of the active fault planes cannot be fully constrained with the available data. The latter is crucial for identifying possible unmapped active faults with an elusive surficial expression, which is important for assessing the area's seismic hazard.

To conclude, the present study provided an overview of seismicity in Central Evia and the Northern Gulf of Evia, with emphasis on several areas that were activated over a relatively short time span. By enhancing the seismic catalog by employing advanced deep-learning models and relocation techniques, it was possible to correlate the activated structures at depth with "suspect" mapped faults and morphological features on the surface. Future research should focus on improving seismic monitoring by densifying the seismological network in the study area to enhance the resolution of the identified active faults and place all these within the broader tectonic setting of the Aegean and mainland Greece extensional domains.

Supplementary Materials: The following supporting information can be downloaded at: https://www.mdpi.com/article/10.3390/geohazards7020038/s1, Figure S1: Location statistics (enhanced dataset with EQT). (a) RMS travel-time residual, (b) formal horizontal and vertical location uncertainties reported by HypoInverse, (c) distribution of the distance to the nearest station with available data, (d) distribution of the relocated focal depths, (e) number of P- and S-wave arrival-times, and (f) azimuthal gap; Figure S2: Location statistics for the initial phases' dataset (before enhancement with EQT). (a) RMS travel-time residual, (b) formal horizontal and vertical location uncertainties reported by HypoInverse, (c) distribution of the distance to the nearest station with available data, (d) distribution of the relocated focal depths, (e) number of P- and S-wave arrival-times, and (f) azimuthal gap.; Figure S3: Arrival-time pick differences between picks derived by the EQ-Transformer (EQT) model and manual picks: (left) for P-waves, and (right) for S-waves. Colors represent different weight classes assigned according to Table S3. P-wave arrival-time differences have a median value of -0.05 s with standard deviation $\sigma = 0.29$ s, while S-wave have median 0.19 s with $\sigma = 0.54$ s. Note that these arrival-time differences are only shown for comparison, as EQT picks have only been used to enhance the dataset with additional picks or to replace previously available automatic P-wave picks. The available manual P or S picks have not been replaced by EQT picks in the final dataset; Figure S4: Initial locations with HypoInverse: (left) with the initial phases dataset, and (right) with the dataset enhanced with EQT. Different colors represent the 8 spatial groups (same as in Figure 2); Figure S5: Cross-section a_1–a_2 (NNW-SSE) (see Figure 4) of initial locations with HypoInverse involving spatial groups #1 (cyan, Drosia) and #2 (yellow, N. Gulf of Evia, southern part): (left) with the initial phases dataset, and (right) with the dataset enhanced with EQT; Figure S6: Cross-section b_1–b_2 (NNW-SSE) (see Figure 5) of initial locations with HypoInverse involving spatial group #8 (red, Psachna): (top) with the initial phases dataset, and (bottom) with the dataset enhanced with EQT. Events with magnitude $M_L \geq 4.3$ are presented with stars.; Figure S7: Cross-section c_1–c_2 (NW–SE) (see Figure 6) of initial locations with HypoInverse involving spatial group #5 (green, Markates–Prokopi): (top) with the initial phases dataset, and (bottom) with the dataset enhanced with EQT. Events with magnitude $M_L \geq 4.3$ are presented with stars.; Figure S8: Cross-section d_1–d_2 (SW–NE) (see Figure 7) of initial locations with HypoInverse involving spatial groups #3 (blue, Mouriki) and #7 (orange, Paralimni): (left) with the initial phases dataset, and (right) with the dataset enhanced with EQT; Figure S9: Multiplet formation diagram, indicating the selection of the optimal correlation threshold (Cth = 0.68). The x-axis represents different trial correlation thresholds. The dark-blue line with square markers indicates the number of formed multiplets (right y-axis), the blue line with circle markers corresponds to the size (number of events, left axis) of the largest multiplet, the green line with asterisks shows the total number of events contained in multiplets, and the black line is the difference between the size of the largest multiplet and the sum of events inside multiplets. The

optimal correlation threshold is chosen at the value which maximizes the black line [34]; Figure S10: Hierarchical clustering dendrogram, formed with nearest neighbor linkage on the cross-correlation matrix. The horizontal red line represents the optimal threshold Cth = 0.68, forming 148 multiplets (shown with different colors) containing a total of 925 events. Table S1: Location statistics per spatial group (enhanced dataset with EQT); Table S2: Location statistics per spatial group (initial phases' dataset); Table S3: Mapping of EQT pick probabilities (pick prob.) to HypoInverse pick weight classes (0–3: best to worst, 4: unused); Table S4: Seismicity rate changes significance tests. Group refers to one of the 8 spatial groups. N_a/N_b, T_a/T_b and λ_a/λ_b are the number of events, the duration (in days) and the seismicity rate (events/day) for periods a/b, respectively.

Author Contributions: Conceptualization, A.K.; methodology, A.K. and V.K.; software, V.K.; validation, A.K., V.K. and G.K.; formal analysis, A.K., V.K., G.K. and H.K.; investigation, A.K., V.K. and N.M.; resources, V.K., G.K. and H.K.; data curation, A.K., V.K. and N.M.; writing—original draft preparation, A.K., V.K., N.M., G.K. and H.K.; writing—review and editing, A.K., V.K., N.M., G.K. and H.K.; visualization, V.K.; supervision, A.K. and G.K. All authors have read and agreed to the published version of the manuscript.

Funding: This research received no external funding.

Data Availability Statement: The data presented in this study are openly available in public databases: the initial catalog and phase arrival-time data from the Seismological Laboratory of the National and Kapodistrian University of Athens (http://www.geophysics.geol.uoa.gr/stations/gmapv3_db/index.php?lang=en, accessed on 26 March 2026). Waveform data from the Hellenic Unified Seismic Network stations are publicly available at the EIDA Node hosted at the National Observatory of Athens (https://eida.gein.noa.gr/, accessed on 26 March 2026). This study uses waveform data from stations of the following networks: HA [9], HL [8], HT [48], HP [49], and 1Y of the AdriaArray project [15]. The focal mechanisms of significant events used herein are from the databases of SL-NKUA (http://www.geophysics.geol.uoa.gr/stations/gmaps3/leaf_significant.php?mapmode=mech&lng=en&year=0, accessed on 26 March 2026) and GI-NOA (https://bbnet.gein.noa.gr/HL/seismicity/mts, accessed on 26 March 2026).

Acknowledgments: We thank the two anonymous reviewers for their constructive comments, which greatly helped to improve the quality of the manuscript. The maps and cross-sections were created using the Generic Mapping Tools (GMT v4.2) software [50].

Conflicts of Interest: The authors declare no conflicts of interest.

References

1. Skouphos, T. Die Swei Grossen Erdbeben in Lokris Am 8/20 Und 15/27 April 1894. *Z. Ges. Erdkd. Berl.* **1894**, *24*, 409–474. (In German)
2. Kouskouna, V.; Sakkas, G.; Cecić, I.; Sakkas, S.; Kaviris, G.; Tertulliani, A. Earthquake Induced Crises: Game Tree Approached Risk Communication and Lessons Learnt. *Ann. Geophys.* **2021**, *64*, SE329. [CrossRef]
3. Ganas, A.; Sokos, E.; Agalos, A.; Leontakianakos, G.; Pavlides, S. Coulomb Stress Triggering of Earthquakes along the Atalanti Fault, Central Greece: Two April 1894 M6+ Events and Stress Change Patterns. *Tectonophysics* **2006**, *420*, 357–369. [CrossRef]
4. Makropoulos, K.; Kaviris, G.; Kouskouna, V. An Updated and Extended Earthquake Catalogue for Greece and Adjacent Areas since 1900. *Nat. Hazards Earth Syst. Sci.* **2012**, *12*, 1425–1430. [CrossRef]
5. Ganas, A.; Mouzakiotis, E.; Moshou, A.; Karastathis, V. Left-Lateral Shear inside the North Gulf of Evia Rift, Central Greece, Evidenced by Relocated Earthquake Sequences and Moment Tensor Inversion. *Tectonophysics* **2016**, *682*, 237–248. [CrossRef]
6. Sakellariou, D.; Rousakis, G.; Kaberi, H.; Kapsimalis, V.; Georgiou, P.; Kanellopoulos, T.; Lykousis, V. Tectono-sedimentary structure and late quaternary evolution of the North Evia gulf basin, Central Greece: Preliminary results. *Bull. Geol. Soc. Greece* **2018**, *40*, 451. [CrossRef]
7. Stucchi, M.; Rovida, A.; Gomez Capera, A.A.; Alexandre, P.; Camelbeeck, T.; Demircioglu, M.B.; Gasperini, P.; Kouskouna, V.; Musson, R.M.W.; Radulian, M.; et al. The SHARE European Earthquake Catalogue (SHEEC) 1000–1899. *J. Seismol.* **2013**, *17*, 523–544. [CrossRef]
8. National Observatory of Athens, Institute of Geodynamics, Athens. Hellenic Unified Seismological Network [Data Set]. International Federation of Digital Seismograph Networks. 1975. [CrossRef]

9. University of Athens. Hellenic Unified Seismological Network [Data Set]. International Federation of Digital Seismograph Networks. 2008. [CrossRef]
10. Caputo, R.; Chatzipetros, A.; Pavlides, S.; Sboras, S. The Greek Database of Seismogenic Sources (GreDaSS): State-of-the-Art for Northern Greece. *Ann. Geophys.* **2013**, *55*, 859–894. [CrossRef]
11. The SHARE Consortium; Woessner, J.; Laurentiu, D.; Giardini, D.; Crowley, H.; Cotton, F.; Grünthal, G.; Valensise, G.; Arvidsson, R.; Basili, R.; et al. The 2013 European Seismic Hazard Model: Key Components and Results. *Bull Earthq. Eng* **2015**, *13*, 3553–3596. [CrossRef]
12. Mousavi, S.M.; Ellsworth, W.L.; Zhu, W.; Chuang, L.Y.; Beroza, G.C. Earthquake Transformer—An Attentive Deep-Learning Model for Simultaneous Earthquake Detection and Phase Picking. *Nat. Commun.* **2020**, *11*, 3952. [CrossRef]
13. Woollam, J.; Münchmeyer, J.; Tilmann, F.; Rietbrock, A.; Lange, D.; Bornstein, T.; Diehl, T.; Giunchi, C.; Haslinger, F.; Jozinović, D.; et al. SeisBench—A Toolbox for Machine Learning in Seismology. *Seismol. Res. Lett.* **2022**, *93*, 1695–1709. [CrossRef]
14. Evangelidis, C.P.; Triantafyllis, N.; Samios, M.; Boukouras, K.; Kontakos, K.; Ktenidou, O.-J.; Fountoulakis, I.; Kalogeras, I.; Melis, N.S.; Galanis, O.; et al. Seismic Waveform Data from Greece and Cyprus: Integration, Archival, and Open Access. *Seismol. Res. Lett.* **2021**, *92*, 1672–1684. [CrossRef]
15. Friederich, W.; Evangelidis, C.; Papazachos, C.; Sokos, E.; Kaviris, G.; Cernih, D. AdriaArray Temporary Network: Greece, North Macedonia [Data Set]. 2026. [CrossRef]
16. Kolínský, P.; Meier, T.; Agius, M.R.; Bijedić, A.; Bokelmann, G.; Borleanu, F.; Brnović, D.; Cambaz, M.D.; Cammarano, F.; Čarman, M.; et al. AdriaArray—A Passive Seismic Experiment to Study Structure, Geodynamics and Geohazards of the Adriatic Plate. *Ann. Geophys.* **2025**, *68*, DM555. [CrossRef]
17. Schlömer, A.; Wassermann, J.; Paffrath, M.; Fischer, K.D.; Friederich, W.; Meier, T.; Cernih, D.; Dedic, J.; Drogreshka, K.; Evangelidis, C.P.; et al. DSEBRA—The German Seismological Broadband Array and Its Contribution to AdriaArray—Deployment and Performance. *Ann. Geophys.* **2025**, *68*, DM560. [CrossRef]
18. Michelini, A.; Cianetti, S.; Gaviano, S.; Giunchi, C.; Jozinović, D.; Lauciani, V. INSTANCE—The Italian Seismic Dataset for Machine Learning. *Earth Syst. Sci. Data* **2021**, *13*, 5509–5544. [CrossRef]
19. Karakonstantis, A. 3-D Simulation of Crust and Upper Mantle Structure in the Broader Hellenic Area through Seismic Tomography. Ph.D. Thesis, Department of Geophysics-Geothermics, Faculty of Geology, University of Athens, Athens, Greece, 2017. (In Greek)
20. Kissling, E.; Ellsworth, W.L.; Eberhart-Phillips, D.; Kradolfer, U. Initial Reference Models in Local Earthquake Tomography. *J. Geophys. Res.* **1994**, *99*, 19635–19646. [CrossRef]
21. Chiarabba, C.; Frepoli, A. Minimum 1D Velocity Models in Central and Southern Italy: A Contribution to Better Constrain Hypocentral Determinations. *Ann. Geophys.* **1997**, *40*, 20. [CrossRef]
22. Klein, F.W. *User's Guide to HYPOINVERSE-2000: A Fortran Program to Solve for Earthquake Locations and Magnitudes*; U.S. Geological Survey Open-File Report 2002-171; U.S. Geological Survey: Reston, VA, USA, 2002; 123p. Available online: https://pubs.usgs.gov/publication/ofr02171 (accessed on 22 March 2026).
23. Elias, P.; Spingos, I.; Kaviris, G.; Karavias, A.; Gatsios, T.; Sakkas, V.; Parcharidis, I. Combined Geodetic and Seismological Study of the December 2020 Mw = 4.6 Thiva (Central Greece) Shallow Earthquake. *Appl. Sci.* **2021**, *11*, 5947. [CrossRef]
24. Kaviris, G.; Kapetanidis, V.; Spingos, I.; Sakellariou, N.; Karakonstantis, A.; Kouskouna, V.; Elias, P.; Karavias, A.; Sakkas, V.; Gatsios, T.; et al. Investigation of the Thiva 2020–2021 Earthquake Sequence Using Seismological Data and Space Techniques. *Appl. Sci.* **2022**, *12*, 2630. [CrossRef]
25. Parginos, D.; Mavrides, A.; Bornovas, I.; Mettos, A.; Katsikatsos, G.; Koukis, G. *Geological Map of Greece: "Khalkis Sheet", 1:50,000*; Institute of Geological and Mineral Exploration: Athens, Greece, 2007.
26. Photiades, A. *Geological Map of Greece: "Steni Dirfyos Sheet", 1:50,000*; Institute of Geological and Mineral Exploration: Athens, Greece, 2018.
27. Katsikatsos, G.; Koukis, G.; Mettos, A. *Geological Map of Greece 1:50,000, "Larymna Sheet"*; Institute of Geological and Mineral Exploration: Athens, Greece, 1978.
28. Caroir, F. Analyse Structurale Du Domaine Nord Eubée: Rifting Plio-Quaternaire et Décrochements Actifs Dans Le Prolongement Occidental de La Faille Nord-Anatolienne (Projet WATER). Ph.D. Thesis, Université de Lille, Lille, France, 2022; 209p.
29. Katsikatsos, G.; Koukis, G.; Fytikas, M.; Anastopoulos, J.; Kanaris, J. *Geological Map of Greece 1:50,000, "Pshachna Sheet", 1:50,000*; Institute of Geological and Mineral Exploration: Athens, Greece, 1981.
30. Tataris, A.; Kounis, G.; Maragoudakis, N. *Geological Map of Greece 1:50,000, "Thivai Sheet", 1:50,000*; Institute of Geological and Mineral Exploration: Athens, Greece, 1970.
31. Palyvos, N.; Bantekas, I.; Kranis, H. Transverse Fault Zones of Subtle Geomorphic Signature in Northern Evia Island (Central Greece Extensional Province): An Introduction to the Quaternary Nileas Graben. *Geomorphology* **2006**, *76*, 363–374. [CrossRef]
32. Waldhauser, F. *HypoDD: A Computer Program to Compute Double-Difference Earthquake Locations*; U.S. Geological Survey Open File Report 2001-113; USGS Publications Warehouse: Reston, VA, USA, 2001; 25p. [CrossRef]

33. Kapetanidis, V.; Deschamps, A.; Papadimitriou, P.; Matrullo, E.; Karakonstantis, A.; Bozionelos, G.; Kaviris, G.; Serpetsidaki, A.; Lyon-Caen, H.; Voulgaris, N.; et al. The 2013 Earthquake Swarm in Helike, Greece: Seismic Activity at the Root of Old Normal Faults. *Geophys. J. Int.* **2015**, *202*, 2044–2073. [CrossRef]
34. Kapetanidis, V. Spatiotemporal Patterns of Microseismicity for the Identification of Active Fault Structures Using Seismic Waveform Cross-Correlation and Double-Difference Relocation. Ph.D. Thesis, University of Athens, Athens, Greece, 2017.
35. Matthews, M.V.; Reasenberg, P.A. Statistical Methods for Investigating Quiescence and Other Temporal Seismicity Patterns. *Pure Appl. Geophys.* **1988**, *126*, 357–372. [CrossRef]
36. Kapetanidis, V.; Karakonstantis, A.; Papadimitriou, P.; Pavlou, K.; Spingos, I.; Kaviris, G.; Voulgaris, N. The 19 July 2019 Earthquake in Athens, Greece: A Delayed Major Aftershock of the 1999 Mw = 6.0 Event, or the Activation of a Different Structure? *J. Geodyn.* **2020**, *139*, 101766. [CrossRef]
37. Kouskouna, V.; Ganas, A.; Kleanthi, M.; Kassaras, I.; Sakellariou, N.; Sakkas, G.; Valkaniotis, S.; Manousou, E.; Bozionelos, G.; Tsironi, V.; et al. Evaluation of Macroseismic Intensity, Strong Ground Motion Pattern and Fault Model of the 19 July 2019 Mw5.1 Earthquake West of Athens. *J. Seismol.* **2021**, *25*, 747–769. [CrossRef]
38. Evangelidis, C.; Fountoulakis, I. Imaging the Western Edge of the Aegean Shear Zone: The South Evia 2022–2023 Seismic Sequence. *Seismica* **2023**, *2*, 1–8. [CrossRef]
39. Spingos, I.; Kaviris, G.; Kapetanidis, V.; Papadimitriou, E.; Vallianatos, F. Shear-Wave Splitting Associated with Fluid Processes beneath Styra, South Euboea: First Results. *Phys. Earth Planet. Inter.* **2024**, *351*, 107196. [CrossRef]
40. Tzanis, A.; Kranis, H.; Chailas, S. An Investigation of the Active Tectonics in Central-Eastern Mainland Greece with Imaging and Decomposition of Topographic and Aeromagnetic Data. *J. Geodyn.* **2010**, *49*, 55–67. [CrossRef]
41. Caroir, F.; Chanier, F.; Gaullier, V.; Sakellariou, D.; Bailleul, J.; Maillard, A.; Paquet, F.; Watremez, L.; Averbuch, O.; Graveleau, F.; et al. Late Quaternary Deformation in the Western Extension of the North Anatolian Fault (North Evia, Greece): Insights from Very High-Resolution Seismic Data (WATER Surveys). *Tectonophysics* **2024**, *870*, 230138. [CrossRef]
42. Sboras, S.; Mouzakiotis, E.; Chousianitis, K.; Karastathis, V.; Evangelidis, C.P.; Lazos, I.; Papageorgiou, A.; Liakopoulos, S.; Iordanidou, K. Where Does the Active North Aegean Sea Shear Stop? Geodynamic and Seismotectonic Implications from Recent Strike-Slip Earthquake Occurrences and GPS-Based Geodetic Analysis in Euboea, Phthiotis and Boeotia, Central Greece. *Tectonophysics* **2025**, *914*, 230917. [CrossRef]
43. Faucher, A.; Gueydan, F.; Jolivet, M.; Alsaif, M.; Célérier, B. Dextral Strike-Slip and Normal Faulting During Middle Miocene Back-Arc Extension and Westward Anatolia Extrusion in Central Greece. *Tectonics* **2021**, *40*, e2020TC006615. [CrossRef]
44. Kranis, H. Neotectonic Basin Evolution in Central-Eastern Mainland Greece: An Overview. *Bull. Geol. Soc. Greece* **2007**, *40*, 360–373. [CrossRef]
45. Kranis, H.D.; Palyvos, N.; Livaditis, G.; Maroukian, H. The Hyambolis Zone: Geomorpho-Logical and Tectonic Evidence of a Transverse Structure in Lokris (Central Greece). *Bull. Geol. Soc. Greece* **2001**, *34*, 251–257. [CrossRef]
46. Roumelioti, Z.; Kiratzi, A. Moderate Magnitude Earthquake Sequences in Central Greece (for the Year 2008). *Bull. Geol. Soc. Greece* **2010**, *43*, 2144–2153. [CrossRef]
47. Jolivet, L.; Faccenna, C.; Huet, B.; Labrousse, L.; Le Pourhiet, L.; Lacombe, O.; Lecomte, E.; Burov, E.; Denèle, Y.; Brun, J.-P.; et al. Aegean Tectonics: Strain Localisation, Slab Tearing and Trench Retreat. *Tectonophysics* **2013**, *597–598*, 1–33. [CrossRef]
48. Aristotle University of Thessaloniki. Hellenic Unified Seismological Network [Data Set]. International Federation of Digital Seismograph Networks, 1981. [CrossRef]
49. University of Patras. Hellenic Unified Seismological Network [Data Set]. International Federation of Digital Seismograph Networks, 2000. [CrossRef]
50. Wessel, P.; Smith, W.H.F. New, Improved Version of Generic Mapping Tools Released. *EoS Trans.* **1998**, *79*, 579. [CrossRef]

Disclaimer/Publisher's Note: The statements, opinions and data contained in all publications are solely those of the individual author(s) and contributor(s) and not of MDPI and/or the editor(s). MDPI and/or the editor(s) disclaim responsibility for any injury to people or property resulting from any ideas, methods, instructions or products referred to in the content.